

Radiative Heat Transfer Flow of Micropolar Fluid with Variable Heat Flux in a Porous Medium

M. M. Rahman, T. Sultana

Department of Mathematics, University of Dhaka
Dhaka-1000, Bangladesh
mansurdu@yahoo.com

Received: 13.12.2006 **Revised:** 15.09.2007 **Published online:** 06.03.2008

Abstract. A two-dimensional steady convective flow of a micropolar fluid past a vertical porous flat plate in the presence of radiation with variable heat flux has been analyzed numerically. Using Darcy-Forchheimer model the corresponding momentum, microrotation and energy equations have been solved numerically. The local similarity solutions for the flow, microrotation and heat transfer characteristics are illustrated graphically for various material parameters. The effects of the pertinent parameters on the local skin friction coefficient, plate couple stress and the heat transfer are also calculated. It was shown that large Darcy parameter leads to decrease the velocity while it increases the angular velocity as well as temperature of the micropolar fluids. The rate of heat transfer in weakly concentrated micropolar fluids is higher than strongly concentrated micropolar fluids.

Keywords: radiation, convection, micropolar fluid, porous medium.

1 Introduction

A micropolar fluid is the fluid with internal structures in which coupling between the spin of each particle and the macroscopic velocity field is taken into account. It is a hydrodynamical framework suitable for granular systems which consist of particles with macroscopic size. The dynamics of micropolar fluids, originated from the theory of Eringen [1] has been a popular area of research. This theory may be applied to explain the flow of colloidal suspensions (Hadimoto and Tokioka [2]), liquid crystals (Lockwood et al. [3]), polymeric fluids, human and animal blood (Ariman et al. [4]) and many other situations.

Ahmadi [5] presented solutions for the flow of a micropolar fluid past a semi-infinite plate taking into account microinertia effects. Soundalgekar and Takhar [6] studied the flow and heat transfer past a continuously moving plate in a micropolar fluid. Gorla [7] studied mixed convection in a micropolar fluid from a vertical surface with uniform heat flux. Rees and Pop [8] studied free convection boundary layer flow of micropolar fluids from a vertical flat plate while Mohammadein and Gorla [9] studied the same

flow bounded by stretching sheet with prescribed wall heat flux, viscous dissipation and internal heat generation. Aissa and Modammedin [10] studied joule heating effects on a micropolar fluid past a stretching sheet with variable electric conductivity. Hassanien et al. [11] studied unsteady magnetohydrodynamic micropolar fluid flow and heat transfer over a vertical porous plate through a porous medium in the presence of thermal and mass diffusion with a constant heat source. Rahman and Sattar [12] studied magnetohydrodynamic convective flow of a micropolar fluid past a vertical porous plate in the presence of heat generation/absorption.

Markin and Mahmood [13] obtained similarity solutions for the mixed convection flow over a vertical plate for the case of constant heat flux condition at the wall. Perdakis and Raptis [14] studied heat transfer of a micropolar fluid in the presence of radiation. Later Raptis [15] studied the same fluid flow past a continuously moving plate in the presence of radiation. Chen and Char [16] have studied the suction and injection on a linearly moving plate subject to uniform wall temperature and heat flux. El-Arabawy [17] studied the effect of suction/injection on a micropolar fluid past a continuously moving plate in the presence of radiation. Ogulu [18] studied the oscillating plate-temperature flow of a polar fluid past a vertical porous plate in the presence of couple stresses and radiation. Recently, Rahman and Sattar [19] studied transient convective heat transfer flow of a micropolar fluid past a continuously moving vertical porous plate with time dependent suction in the presence of radiation.

In the present work we investigate the thermal radiation interaction of the boundary layer flow of micropolar fluid past a heated vertical porous plate embedded in a porous medium with variable suction as well as heat flux at the plate. The local similarity solutions are then obtained numerically for various parameters entering into the problem using shooting method and discussed the results from the physical point of view.

2 Mathematical formulation

Let us consider a steady two-dimensional flow of a viscous, incompressible micropolar fluid of temperature T_∞ past a heated vertical porous flat plate immersed in a porous medium and there is a suction velocity $v_0(x)$ at the plate. Consider a variable surface heat flux such that the temperature at the surface of the plate is proportional to x^m (x measures the distance from the leading edge along the surface of the plate and m is a constant). The flow is assumed to be in the x -direction, which is taken along the plate in the upward direction and y -axis is normal to it. The flow configuration and the coordinate system are shown in the Fig. 1.

The fluid is considered to be gray; absorbing-emitting radiation but non-scattering medium and the Rosseland approximation is used to describe the radiative heat flux in the energy equation. The radiative heat flux in the x -direction is considered negligible in comparison to the y -direction.

Within the framework of the above-noted assumptions, we assume that the Boussinesq and boundary layer approximations hold and using the Darcy-Forchheimer model,

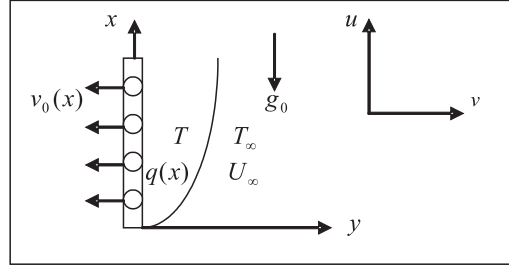


Fig. 1. Flow configuration and coordinate system.

the governing equations relevant to the problem in the presence of radiation are given by:

$$\frac{\partial u}{\partial x} + \frac{\partial v}{\partial y} = 0, \quad (1)$$

$$u \frac{\partial u}{\partial x} + v \frac{\partial u}{\partial y} = \nu_a \frac{\partial^2 u}{\partial y^2} + \frac{S}{\rho} \frac{\partial \sigma}{\partial y} + g_0 \beta (T - T_\infty) - \frac{\nu_a}{K'} (u - U_\infty) - \frac{b}{K'} (u - U_\infty)^2, \quad (2)$$

$$u \frac{\partial \sigma}{\partial x} + v \frac{\partial \sigma}{\partial y} = \frac{\nu_s}{\rho j} \frac{\partial^2 \sigma}{\partial y^2} - \frac{S}{\rho j} \left(2\sigma + \frac{\partial u}{\partial y} \right), \quad (3)$$

$$u \frac{\partial T}{\partial x} + v \frac{\partial T}{\partial y} = \frac{k}{\rho c_p} \frac{\partial^2 T}{\partial y^2} - \frac{1}{\rho c_p} \frac{\partial q_r}{\partial y}, \quad (4)$$

where u, v are the velocity components along x, y co-ordinates respectively, $\nu_a = \frac{\mu + S}{\rho}$ is the apparent kinematic viscosity, μ is the coefficient of dynamic viscosity, S is the microrotation coupling coefficient (also known as the coefficient of gyro-viscosity or as the vortex viscosity), ρ is the mass density of the fluid, σ is the microrotation component normal to the xy -plane, b is the empirical constant, K' is the Darcy permeability, $\nu_s = (\mu + \frac{S}{2})j$ (see Rees and Bassom [20]) is the microrotation viscosity or spin-gradient viscosity, j is the micro-inertia density, T is the temperature of the fluid in the boundary layer, T_∞ is the temperature of the fluid outside the boundary layer, U_∞ is the velocity of the fluid far away from the plate, c_p is the specific heat of the fluid at constant pressure, k is the thermal conductivity, q_r is the radiative heat flux, g_0 is the acceleration due to gravity, β is the volumetric coefficient of thermal expansion.

By using Rosseland approximation (see Raptis [15]), q_r takes the form

$$q_r = -\frac{4\sigma_1}{3k_1} \frac{\partial T^4}{\partial y}, \quad (5)$$

where σ_1 , the Stefan-Boltzmann constant and k_1 is the mean absorption coefficient.

We assume that the temperature differences within the flow are sufficiently small such that T^4 may be expressed as a linear function of temperature. This is accomplished

by expanding T^4 in a Taylor's series about T_∞ and neglecting higher-order terms, thus

$$T^4 \cong T_\infty^4 + (T - T_\infty) \cdot 4T_\infty^3 = 4T_\infty^3 T - 3T_\infty^4. \quad (6)$$

By using (5) and (6) equation (4) gives

$$u \frac{\partial T}{\partial x} + v \frac{\partial T}{\partial y} = \frac{k}{\rho c_p} \frac{\partial^2 T}{\partial y^2} + \frac{16\sigma_1 T_\infty^3}{3\rho c_p \kappa_1} \frac{\partial^2 T}{\partial y^2}. \quad (7)$$

The corresponding boundary conditions for the above problem are given by,

$$\begin{aligned} u = 0, \quad v = v_0(x), \quad \sigma = -n \frac{\partial u}{\partial y}, \quad -\kappa \left(\frac{\partial T}{\partial y} \right) = q_w(x) = b_0 x^m \quad \text{at } y = 0, \\ u = U_\infty, \quad \sigma = 0, \quad T = T_\infty \quad \text{as } y \rightarrow \infty. \end{aligned} \quad (8)$$

Positive and negative values for v_0 indicate blowing and suction respectively, while $v_0 = 0$ corresponds to an impermeable plate. When microrotation parameter $n = 0$ we obtain $\sigma = 0$ which represents no-spin condition i.e. the microelements in a concentrated particle flow-close to the wall are not able to rotate as stated by Jena and Mathur [21]. The case $n = 0.5$ represents vanishing of the anti-symmetric part of the stress tensor and represents weak concentration. For this case Ahmadi [5] suggested that in a fine particle suspension the particle spin is equal to the fluid velocity at the wall. The case corresponding to $n = 1$ be representative of turbulent boundary layer flows (see Peddison and McNitt [22]). In equation (8), the last condition represents non-uniform heat flux at the surface of the plate.

3 Transformations of the model

In order to obtain local similarity solution of the problem we adopted the following non-dimensional variables which have been used by many authors in the literature (see for example [12, 15, 17]):

$$\eta = y \sqrt{\frac{U_\infty}{2\nu_a x}}, \quad \psi = \sqrt{2\nu_a U_\infty x} f(\eta), \quad \sigma = y \sqrt{\frac{U_\infty^3}{2\nu_a x}} g(\eta), \quad (9)$$

where ψ is the stream function. Since $u = \frac{\partial \psi}{\partial y}$ and $v = -\frac{\partial \psi}{\partial x}$ we have from equation (9) that

$$u = U_\infty f' \quad \text{and} \quad v = -\sqrt{\frac{\nu_a U_\infty}{2x}} (f - \eta f'). \quad (10)$$

Here f is non-dimensional stream function and prime denotes differentiation with respect to η .

The thermal boundary conditions depend on the type of heating process being considered, that is the prescribed heat flux. Define the temperature distribution as follows

$$T - T_\infty = \frac{D}{k} \sqrt{\frac{2\nu_a x}{U_\infty}} \left(\frac{x}{L} \right)^2 \theta(\eta), \quad (11)$$

where D is a constant and L is some characteristic length.

Now substituting equations (9)–(11) into equations (2), (3) and (7) we obtain the following non-dimensional ordinary differential equations which are locally similar as some of the parameters depend on the local coordinate x ,

$$f''' + f f'' + K g' + 2\gamma\theta - 2\lambda(f' - 1) - F_s(f' - 1)^2 = 0, \quad (12)$$

$$G_2 g'' - 2G_1(2g + f'') + f'g + g'f = 0, \quad (13)$$

$$\theta'' + Pn f \theta' - 5Pn f' \theta = 0, \quad (14)$$

where $K = \frac{S}{\rho\nu_a}$ is the coupling parameter, $\gamma = \left(\frac{2Gr_x^2}{Re_x}\right)^{\frac{1}{2}}$ is the local buoyancy parameter, $Gr_x = \frac{g_0\beta b_0 x^4}{\kappa U_\infty^2}$ is the modified Grashof number, $Re_x = \frac{U_\infty x}{\nu_a}$ is the local Reynolds number, $\lambda = \frac{1}{Da}$ is the Darcy parameter, $Da = \frac{K' U_\infty}{\nu_a x}$ is the modified Darcy number, $F_s = \frac{bx}{K'}$ is the modified Forchheimer number, $G_1 = \frac{Sx}{\rho j U_\infty}$ is the vortex viscosity parameter, $G_2 = \frac{\nu_s}{\rho j \nu_a}$ is the spin gradient viscosity parameter, $Pn = \frac{3NP_r}{3N+4}$ is the radiative Prandtl number, $N = \frac{kk_1}{4\sigma_1 T_\infty^3}$ is the radiation parameter, $Pr = \frac{\rho\nu_a c_p}{k}$ is the Prandtl number.

The transformed thermal boundary conditions may be written as

$$\theta'(0) = -\frac{b_0}{D} L^2 x^{m-2}, \quad \theta'(\infty) = 0. \quad (15)$$

But as $\theta'(0)$ must be equal to -1 , this implies (as could be concluded from equation (15)) that $m = 2$ and b_0 should satisfy the relation $b_0 = \frac{D}{L^2}$.

Then the corresponding boundary conditions (8) become,

$$\begin{aligned} f = V_0, \quad f' = 0, \quad g = -n f'', \quad \theta' = -1 \quad \text{at } \eta = 0, \\ f' = 1, \quad g = 0, \quad \theta = 0 \quad \text{as } \eta \rightarrow \infty, \end{aligned} \quad (16)$$

where $V_0 = -v_0 \sqrt{\frac{2x}{\nu_a U_\infty}}$ is the suction velocity at the plate for $V_0 > 0$.

4 Skin friction coefficient, plate couple stress and Nusselt number

The quantities of chief physical interest are the skin friction coefficient, plate couple stress and the Nusselt number (rate of heat transfer). The equation defining the wall shear stress is

$$\tau_w = (\mu + S) \left(\frac{\partial u}{\partial y} \right)_{y=0} + S(\sigma)_{y=0}. \quad (17)$$

The local skin friction coefficient is defined as

$$C_f = \frac{\tau_w}{\frac{1}{2}\rho U_\infty^2} = (2Re_x^{-1})^{\frac{1}{2}} [f''(0) + Kg(0)] = (2Re_x^{-1})^{\frac{1}{2}} (1 - nK)f''(0). \quad (18)$$

Thus from equation (18) we see that the local values of the skin friction coefficient C_f is proportional to $f''(0)$.

The equation defining the plate couple stress is

$$M_w = \nu_s \left(\frac{\partial \sigma}{\partial y} \right)_{y=0}. \quad (19)$$

The dimensionless couple stress is defined by

$$M_x = \frac{M_w}{\frac{1}{2} \rho \nu_a U_\infty} = \frac{G_2 K}{G_1} g'(0). \quad (20)$$

Thus the local couple stress in the boundary layer is proportional to $g'(0)$.

We may define a non-dimensional coefficient of heat transfer, which is known as Nusselt number as follows:

$$Nu_x = \frac{xh(x)}{k}, \quad (21)$$

where $h(x) = \frac{q_w(x)}{T_w - T_\infty}$ and $q_w(x) = -\kappa \left(\frac{\partial T}{\partial y} \right)_{y=0} - \frac{4\sigma_1}{3\kappa_1} \left(\frac{\partial T^4}{\partial y} \right)_{y=0}$ is the quantity of heat transferred through unit area. Now the rate of heat transfer, in terms of the dimensionless Nusselt number, given by

$$Nu_x = (2^{-1} Re_x)^{\frac{1}{2}} \left(1 + \frac{4}{3N} \right) \frac{1}{\theta(0)}. \quad (22)$$

Thus from equation (22) we see that the local Nusselt number Nu_x is reciprocal to $\theta(0)$. Hence the numerical values proportional to C_f , M_x and Nu_x are calculated from equations (18), (20) and (22) are shown in Figs. 10–12.

5 Numerical solution

The set of nonlinear ordinary differential equations (12)–(14) with boundary conditions (16) have been solved by using sixth order Runge-Kutta method along with Nachtsheim-Swigert [23] shooting iteration technique with $V_0, \gamma, K, \lambda, Fs, G_1, G_2, Pn$ and n as prescribed parameters. A step size of $\Delta\eta = 0.001$ was selected to be satisfactory for a convergence criterion of 10^{-6} in all cases. The value of η_∞ was found to each iteration loop by the statement $\eta_\infty = \eta_\infty + \Delta\eta$. The maximum value of η_∞ , to each group of parameters $V_0, \gamma, K, \lambda, Fs, G_1, G_2, Pn$ and n is determined when the value of the unknown boundary conditions at $\eta = 0$ not change to successful loop with error less than 10^{-6} .

In order to verify the effects of the step size $\Delta\eta$ we ran the code for our model with three different step sizes as $\Delta\eta = 0.01$, $\Delta\eta = 0.001$, and $\Delta\eta = 0.005$ and in each case we found excellent agreement among them. Fig. 2(a)–(c), respectively, shows the velocity, microrotation and temperature profiles for different step sizes.

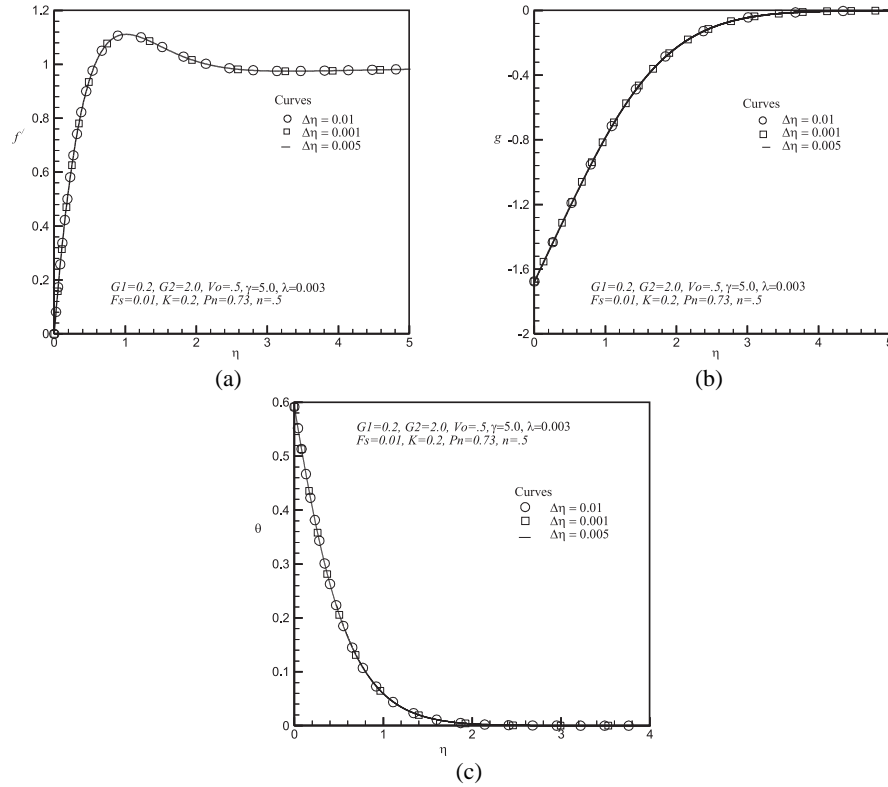


Fig. 2. (a) Velocity profiles for different $\Delta\eta$; (b) microrotation profiles for different $\Delta\eta$; (c) temperature profiles for different $\Delta\eta$.

To assess the accuracy of our code, we reproduced the values of $f''(0)$, $g'(0)$ and $-\theta'(0)$ which are proportional respectively to the local skin friction coefficient, plate couple stress and the rate of heat transfer coefficient considering the model of El-Arabawy [17]. Tables 1–3 show the comparison of the data produced by our code and that of El-Arabawy. In fact the results show a close agreement, hence an encouragement for the use of the present code for our model.

Table 1. Comparison of $f''(0)$ for $Pr = 0.733$, $N = 5.0$

v_0	Code El-Arabawy [17]	Present code
-0.7	-0.278827	-0.278390
-0.2	-0.504059	-0.503800
0.0	-0.616542	-0.616237
0.2	-0.741521	-0.741131
0.7	-1.099430	-1.098857

Table 2. Comparison of $g'(0)$ for $Pr = 0.733$, $N = 5.0$

v_0	Code El-Arabawy [17]	Present code
-0.7	0.236917	0.236511
-0.2	0.321165	0.320745
0.0	0.355330	0.355138
0.2	0.389278	0.389055
0.7	0.468923	0.468660

Table 3. Comparison of $-\theta'(0)$ for $Pr = 0.733$, $N = 5.0$

v_0	Code El-Arabawy [17]	Present code
-0.7	0.247513	0.242280
-0.2	0.370236	0.367887
0.0	0.427013	0.429061
0.2	0.492675	0.496532
0.7	0.686869	0.689726

6 Results and discussion

The present work generalized the problem of heating effects on a boundary layer of a micropolar fluid over the porous plate with variable heat flux in the presence of radiation. For the purpose of discussing the results, the numerical calculations are presented in the form of non-dimensional velocity, microrotation and temperature profiles. In the calculations the values of the local buoyancy parameter γ , coupling parameter K , suction parameter V_0 , radiative Prandtl number Pr , Darcy parameter λ , Forchheimer number Fs , vortex viscosity parameter G_1 , and spin-gradient viscosity parameter G_2 are chosen arbitrarily to carryout the parameter survey. The case $\gamma \gg 1$ corresponds to free convection, $\gamma = 1$ corresponds to mixed convection and $\gamma \ll 1$ corresponds to forced convection. The existence of the free convection current is due to the difference in temperature of the plate T_w and the temperature in the uniform flow, viz. $T_w - T_\infty$. Hence the difference may be positive, zero or negative depending upon $T_w > T_\infty$. Then the values of γ will assume positive, zero or negative values. Physically $\gamma < 0$ corresponds to as externally heated plate as the free convection currents are carried towards the plate and $\gamma > 0$ corresponds to an externally cooled plate while $\gamma = 0$ corresponds to the absence of free convection currents. Since we are considering cooling problem, only positive values of γ are chosen.

Fig. 3(a) shows the velocity profiles for different values of suction parameter V_0 for a cooling plate. It can be seen that for cooling of the plate the velocity profiles decrease monotonically with the increase of suction parameter indicating the usual fact that suction stabilizes the boundary layer growth. The free convection effect is also apparent in this figure. For a fixed suction velocity V_0 , velocity is found to increase and reaches a maximum value in a region close to the plate, then gradually decreases

to one. Fig. 3(b) shows the microrotation (angular velocity) profiles for different values of suction parameter. The angular velocity g remains negative and decreases with the increase of V_0 close to the plate where viscosity is dominant. After a short distance from the plate ($\eta \approx 0.2$) these profiles overlap and then increase with the increase of V_0 . Within the boundary layer region these profiles increase from $-\frac{1}{2}f''(0)$ to zero as η increases from zero to infinity. Fig. 3(c) indicates the temperature profiles showing the effect of suction parameter V_0 . It can be seen that temperature decreases with the increase of suction. Decelerated fluid particles close to the heated wall absorb more heat from the plate as a consequence the temperature of the fluid within the boundary layer increases. But when these decelerated fluid particles are sucked through the porous plate there is decrease to the temperature profile.

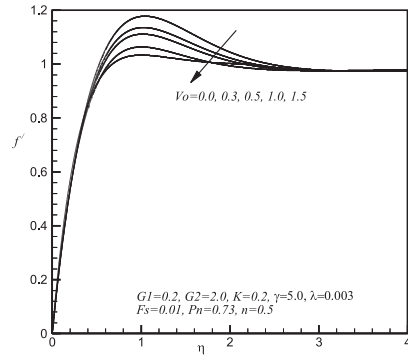
Fig. 4(a) shows the velocity profiles for different values of coupling parameter K . From this figure we see that for cooling plate velocity increases with the increase of the coupling parameter K . Fig. 4(b) shows the effect of coupling parameter in the microrotation profiles. From this figure we observe that microrotation decreases monotonically as the increase of K . Fig. 4(c) shows the decreasing effect of coupling parameter on the temperature profiles.

The effect of modified Forchheimer number Fs on the velocity field is shown in Fig. 5(a). From this figure we see that velocity decreases with the increase of Fs . Fig. 5(b) shows the effect of Fs in the microrotation profiles. From this figure we observe that Fs has increasing effect on the microrotation profiles. Forchheimer number has also increasing effect on the temperature profiles which is shown in the Fig. 5(c).

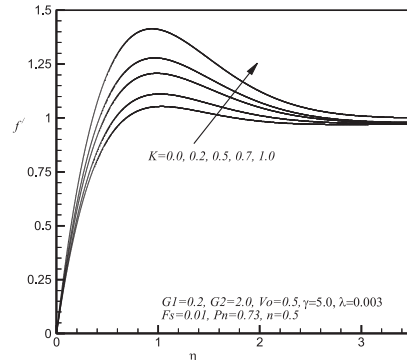
The effect of the local Darcy parameter λ on the velocity field is shown in the Fig. 6(a). From this figure we observe that velocity profiles decrease with the increase of λ . Darcy number is the measurement of the porosity of the medium, as the porosity of the medium increases, the value of Da increases and hence λ decreases. For large porosity of the medium fluid gets more space to flow, consequently fluid velocity increases. The case $\lambda = 0$ corresponds to a pure fluid, rather than a porous medium. Fig. 6(b) shows that microrotation increases with the increase of Darcy parameter λ . The effect of λ on the temperature profiles is shown in Fig. 6(c). From here we see that temperature profiles increase with the increase of Darcy parameter.

Fig. 7(a) shows the effect of vortex viscosity parameter G_1 on the velocity profiles for cooling plate. From here we see minor decreasing effect of G_1 on the velocity profiles. Fig. 7(b) shows the effect of G_1 on the microrotation profiles. From this figure we see that microrotation increases very rapidly with the increase of the vortex viscosity parameter G_1 . It is also understood that as the vortex viscosity increases the rotation of the micropolar constituents gets induced in most part of the boundary layer except very close to the wall where kinematic viscosity dominates the flow. From Fig. 7(c) we found no effect of G_1 on temperature profiles.

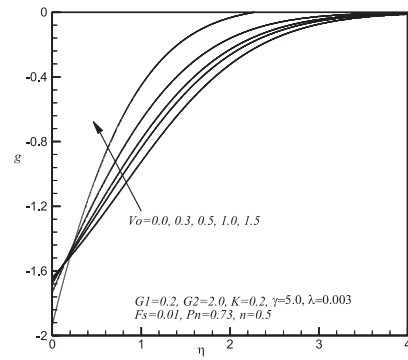
In Fig. 8(a)–(c), respectively, we have varied the spin-gradient viscosity parameter G_2 keeping all other parameters value fixed. From Fig. 8(a) we see that velocity profiles increase slowly with the increase of spin-gradient viscosity parameter G_2 . The effect of G_2 is significant on the microrotation profiles. From Fig. 8(b) we see that microrotation decreases very rapidly with the increase of the spin-gradient viscosity parameter.



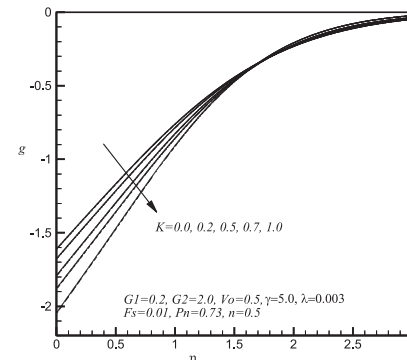
(a)



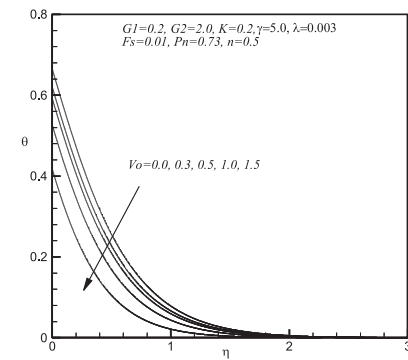
(a)



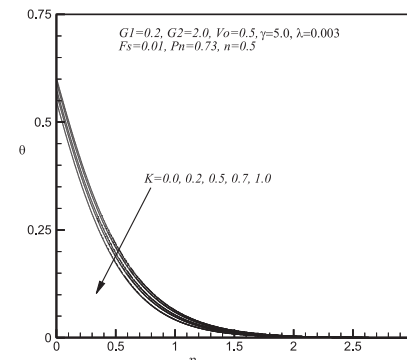
(b)



(b)



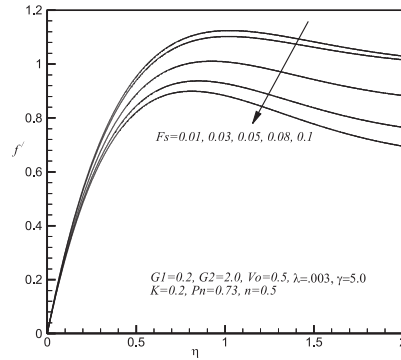
(c)



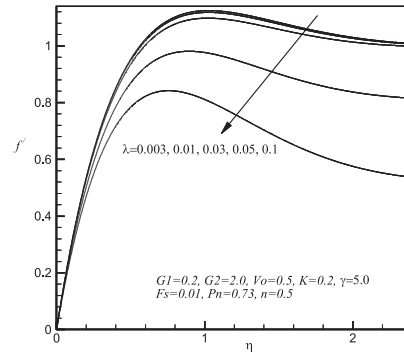
(c)

Fig. 3. Variations of non-dimensional (a) velocity, (b) microrotation and (c) temperature profiles for different values of V_o .

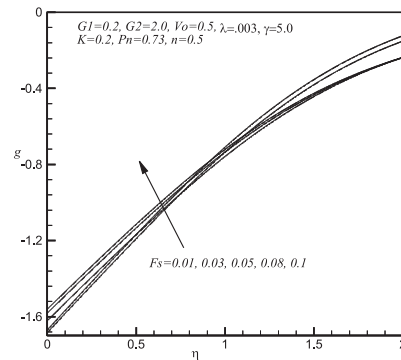
Fig. 4. Variations of non-dimensional (a) velocity, (b) microrotation and (c) temperature profiles for different values of K .



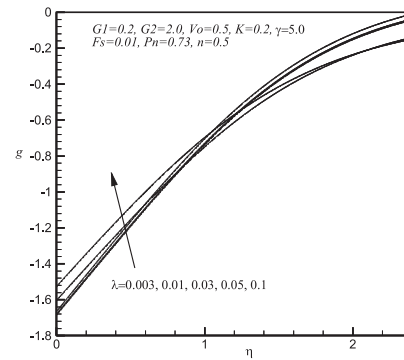
(a)



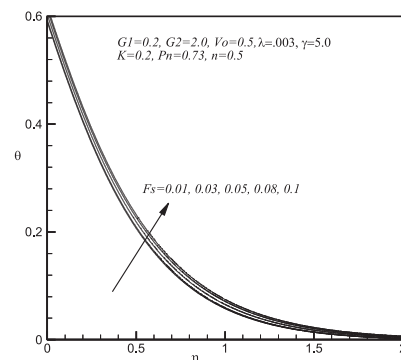
(a)



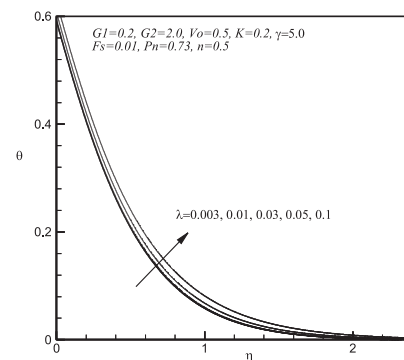
(b)



(b)



(c)



(c)

Fig. 5. Variations of non-dimensional (a) velocity, (b) microrotation and (c) temperature profiles for different values of F_s .

Fig. 6. Variations of non-dimensional (a) velocity, (b) microrotation and (c) temperature profiles for different values of λ .

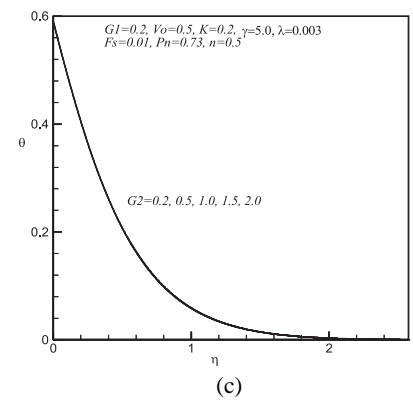
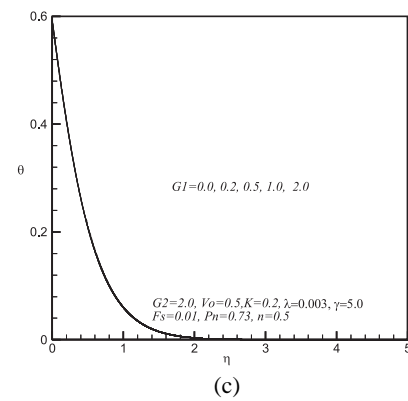
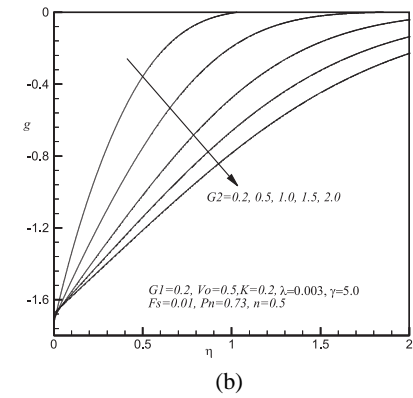
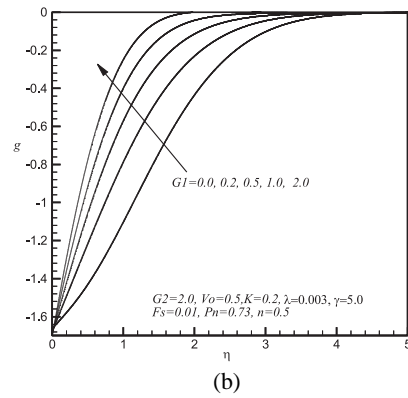
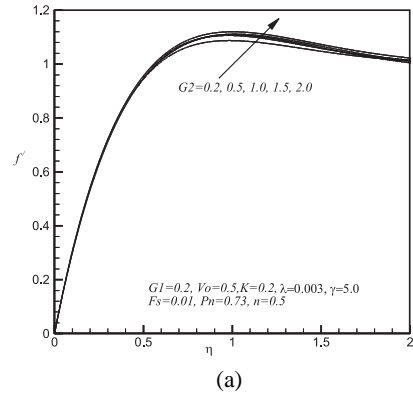
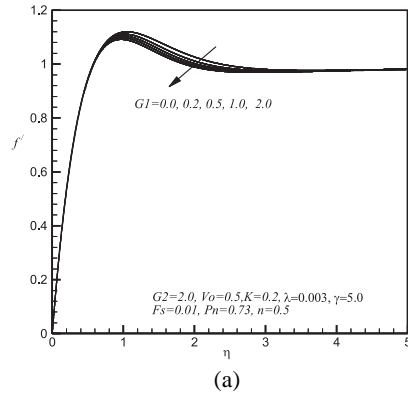
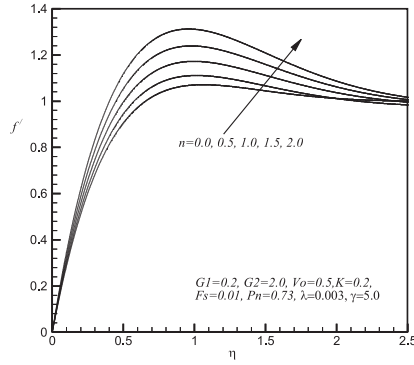
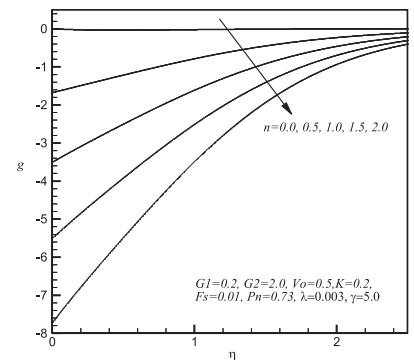


Fig. 7. Variations of non-dimensional (a) velocity, (b) microrotation and (c) temperature profiles for different values of G_1 .

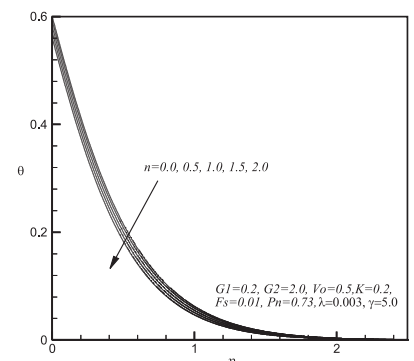
Fig. 8. Variations of non-dimensional (a) velocity, (b) microrotation and (c) temperature profiles for different values of G_2 .



(a)

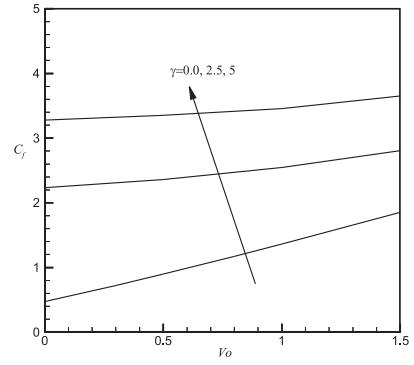


(b)

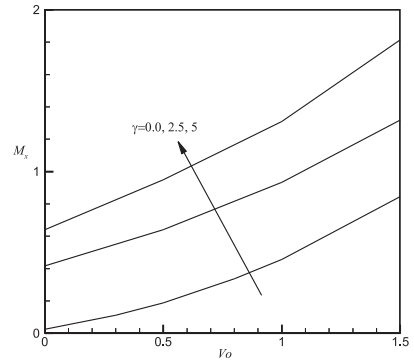


(c)

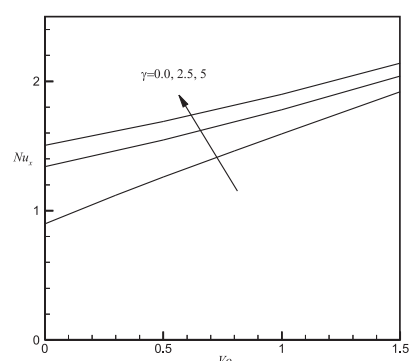
Fig. 9. Variations of non-dimensional (a) velocity, (b) microrotation and (c) temperature profiles for different values of n .



(a)



(b)



(c)

Fig. 10. Variations of (a) local skin friction coefficient, (b) rate of coupling and (c) Nusselt number for different values of γ and V_0 .

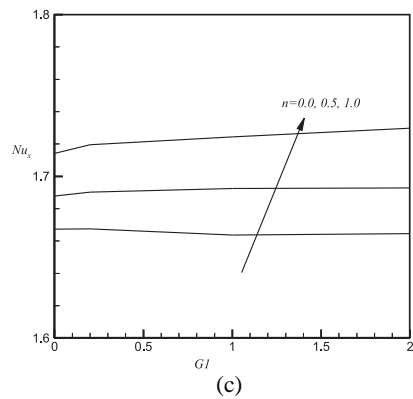
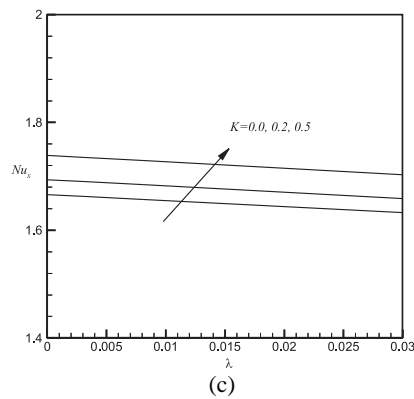
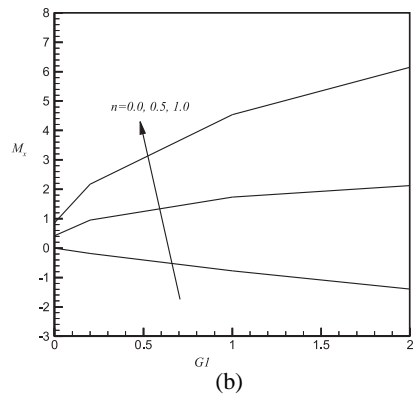
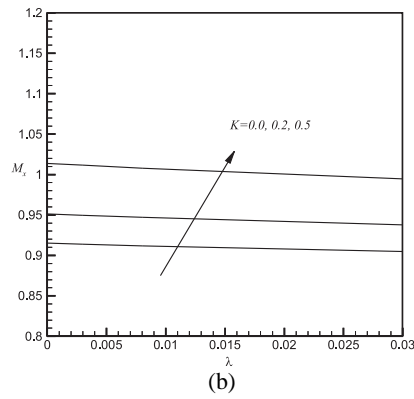
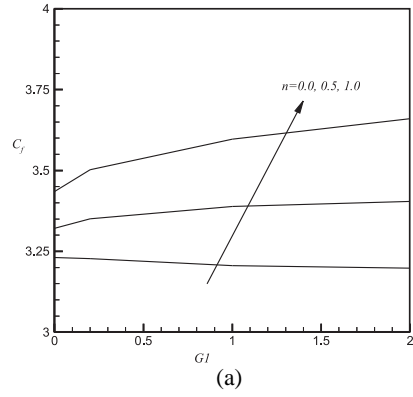
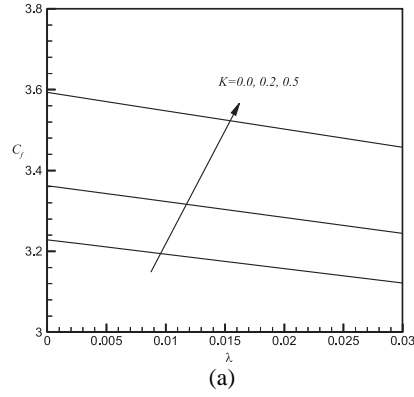


Fig. 11. Variations of (a) local skin friction coefficient, (b) rate of coupling and (c) Nusselt number for different values of λ and K .

Fig. 12. Variations of (a) local skin friction coefficient, (b) rate of coupling and (c) Nusselt number for different values of n and G_1 .

From Fig. 8(c) we see that the values of G_2 introduce no effect on the temperature profiles.

The above-mentioned calculations have been done for a weakly concentrated micropolar fluid i.e. for the microrotation parameter $n = 0.5$. Here we have varied the microrotation parameter n , keeping all other parameters value fixed. Fig. 9(a) reveals that as n increases the concentration of the fluid decreases hence fluid velocity increases. Fig. 9(b) shows the microrotation profiles for different values of n . Microrotation decreases significantly with the increase of n . We observe that g increases from $-nf''(0)$ to zero as n increases from zero to infinity. From Fig. 9(c) we observe that temperature decreases as we go from strong concentration fluid to weak concentration fluid.

In Fig. 10(a)–(c), respectively, we have presented the physical parameters skin friction coefficients, plate couple stress and the rate of heat transfer for different values of the local buoyancy parameter γ and suction parameter V_0 . From these figures we see that skin friction C_f , plate couple stress M_x and Nusselt number Nu_x increases rapidly with the increase of γ as well as with V_0 .

Fig. 11(a)–(c), respectively, show the skin friction coefficients, plate couple stress and the rate of heat transfer for different values of coupling parameter K and Darcy parameter λ . Here we found skin friction, plate couple stress and Nusselt number increase with the increase of K and decrease with the increase of λ .

The effect of microrotation parameter n and vortex viscosity parameter G_1 on the skin friction, plate couple stress and the rate of heat transfer are shown in Fig. 12(a)–(c), respectively. In these figures we found that skin friction, plate couple stress and Nusselt number increases with the increase of n for a fixed value of G_1 . From these figures it is also clear that C_f , M_x and Nu_x increases with the increase of G_1 except for the case $n = 0$. For $n = 0$, C_f and M_x decreases while Nu_x oscillates with the increase of G_1 .

7 Conclusions

In this paper, we have investigated numerically the radiative heat transfer flow of micropolar fluid past a vertical permeable flat plat embedded in a porous medium varying surface heat flux. Using usual similarity transformations the governing equations have been transformed into non-linear ordinary differential equations and were solved for similar solutions by using Nachtsheim-Swigert shooting iteration technique. Effects of the various parameters such as the local buoyancy parameter γ , coupling parameter K , suction parameter V_0 , local Darcy parameter λ , local Forchheimer number Fs , local vortex viscosity parameter G_1 , and spin-gradient viscosity parameter G_2 on the flow, microrotation, and temperature profiles are examined. The following conclusions can be drawn as a result of the numerical computations:

1. Skin friction coefficient increases with the increase of suction parameter, buoyancy parameter, coupling parameter, non-zero microrotation parameter and spin gradient viscosity parameter except for no spin condition, $n = 0$. This coefficient decreases with the increase of the Darcy parameter.

2. Plate couple stress increases with the increase of suction parameter, buoyancy parameter, coupling parameter, and non-zero microrotation parameter.
3. The rate of heat transfer increases with the increase of the suction parameter, buoyancy parameter, coupling parameter and non-zero microrotation parameter.
4. Large Darcy parameter leads to the decrease of the velocity profiles and increase of the microrotation as well as temperature profiles.
5. Radiation has significant decreasing effect on the velocity and temperature field while it has increasing effect on the angular velocity.

Acknowledgement

We would like to thank the anonymous referees for their very expertise comments for the further improvement of the paper.

References

1. A. C. Eringen, Theory of micropolar fluids, *J. Math. Mech.*, **16**, pp. 1–18, 1966.
2. B. Hadimoto, T. Tokioka, Two-dimensional shear flows of linear micropolar fluids, *Int. J. Eng. Sci.*, **7**, pp. 515–522, 1969.
3. F. Lockwood, M. Benchaitra, S. Friberg, *Study of polytropic liquid crystals in viscometric flow and elastohydrodynamic contact ASLE Tribology Trans.*, **30**, pp. 539–548, 1987.
4. T. Ariman, M. A. Turk, N. D. Sylvester, Microcontinuum fluid mechanics – a review, *Int. J. Eng. Sci.*, **12**, pp. 273–293, 1974.
5. G. Ahmadi, Self-similar solution of incompressible micropolar boundary layer flow over a semi- infinite plate, *Int. J. Eng. Sci.*, **14**, pp. 639–646, 1976.
6. V. M. Soundalgekar, H. S. Takhar, Flow of a micropolar fluid on a continuous moving plat, *Int. J. Eng. Sci.*, **21**, p. 961, 1983.
7. R. S. R. Gorla, Mixed convection in a micropolar fluid from a vertical surface with uniform heat flux, *Int. J. Eng. Sci.*, **30**, pp. 349–358, 1992.
8. D. A. S. Rees, I. Pop, Free convection boundary layer flow of micropolar fluid from a vertical flat plat, *IMA J. Appl. Math.*, **61**, pp. 179–197, 1998.
9. A. A. Mohammadein, R. S. R. Gorla, Heat transfer in a micropolar fluid over a stretching sheet with viscous dissipation and internal heat generation, *Int. J. Num. Meth., Heat Fluid Flow.*, **11**(1), pp. 50–58, 2001.
10. W. A. Aissa, A. A. Mohammadein, Joule heating effects in a micropolar fluid past a stretching sheet with variable electric conductivity, *J. Comput. Appl. Mech.*, **6**, pp. 3–13, 2005.

11. I. A. Hassanien, F.S. Ibrahim, A. A. Bakr, Unsteady magnetohydrodynamic micropolar fluid flow and heat transfer over a vertical porous plate through a porous medium in the presence of thermal and mass diffusion with a constant heat source, *Canadian J. Phys.*, **82**(10), pp. 775–790, 2004.
12. M. M. Rahman, M. A. Sattar, Magneto hydrodynamic convective flow of a micropolar fluid past a continuously moving vertical porous plate in the presence of heat generation/absorption, *ASME J. H. Transfer*, **128**, pp. 142–152, 2006.
13. J. H. Markin, T. Mahmood, Mixed convection boundary layer similarity solution, prescribed heat flux, *ZAMP*, **40**, pp. 61–68, 1989.
14. C. Perdikis, A. Raptis, Heat transfer of a micropolar fluid by the presence of radiation, *Heat Mass Transfer*, **31**, pp. 381–382, 1996.
15. A. Raptis, Flow of a micropolar fluid past a continuously moving plate by the presence of radiation, *Int. J. Heat Mass Transfer*, **41**, pp. 2865–2866, 1998.
16. C. K. Chen, N. I. Char, Heat transfer of a continuous stretching surface with suction or blowing, *J. Math. Anal. Appl.*, **135**, pp. 568–580, 1988.
17. H. A. M. El-Arabawy, Effect of suction/injection on the flow of a micropolar fluid past a continuously moving plate in the presence of radiation, *Int. J. Heat Mass Transfer*, **46**, pp. 1471–1477, 2003.
18. A. Ogulu, On the oscillating plate-temperature flow of a polar fluid past a vertical porous plate in the presence of couple stresses and radiation, *Int. comm. Heat Mass Transfer*, **32**, pp. 1231–1243, 2005.
19. M. M. Rahman, M. A. Sattar, Transient convective flow of micropolar fluid past a continuously moving vertical porous plate in the presence of radiation, *Int. J. App. Mech. Engi.*, **12**(2), pp. 497–513, 2007.
20. D. A. S. Rees, A. P. Bassom, The Blasius boundary-layer flow of a micropolar fluid, *Int. J. Engi. Sci.*, **34**, pp. 113–124, 1966.
21. S. K. Jena, M. N. Mathur, Similarity solution for laminar free convection flow of thermo-micropolar fluid past a non-isothermal vertical flat plate, *Int. J. Engi. Sci.*, **19**, pp. 1431–1439, 1981.
22. J. Peddison, R. P. McNitt, Boundary layer theory for micropolar fluid, *Recent Adv. Engi. Sci.*, **5**, pp. 405–426, 1970.
23. P.R. Nachtsheim, P. Swigert, Satisfaction of the asymptotic boundary conditions in numerical solution of the system of non-linear equations of boundary layer type, NASSA TND-3004, 1965.